nature communications

Article

https://doi.org/10.1038/s41467-026-69048-1

Solution-synthesized stable triaza[4] triangulene triradical with a quartet ground state

Received: 9 December 2025

Accepted: 20 January 2026

Published online: 03 February 2026

Check for updates

Xudong Bai[1,4], Di Zhang[1,4], Yushuang Zhang[2], Yihan Wang[1], Yanning Cheng[1], Yi Xie[2], Ziqi Zhu[1], Shang-Da Jiang[2,3] ✉ & Dahui Zhao[1] ✉

As a renowned class of open-shell molecules characterized by triangular nanographenic structures and novel magnetic properties with high-spin ground states, triangulenes are attractive targets to both synthetic chemists and molecular magnet researchers. Here, a highly stable aza-derivative of [4] triangulene triradical (**1**) is achieved, with a quartet ground state ($S = 3/2$). By virtue of the stability under ambient conditions ($\tau_{1/2}$ ~ 9 days in the solid state and 28 h in an air-saturated solution), thorough structural and magnetic characterizations are performed. Crystallographic analysis confirms that **1** has a planar triangular polycyclic aromatic skeleton embedded with delocalized spins. Concurrently, continuous-wave and pulsed EPR spectroscopies provide unambiguous evidence supporting its high-spin ground state. SQUID measurements reveal impressively large doublet-quartet energy gap ($\Delta E_{D\text{-}Q} = 3.18$ kcal/mol), indicating very strong intramolecular ferromagnetic spin-spin exchanges ($J/k_B = +534$ K) rendered by the triangulene structure.

In the past few years, organic radicals have witnessed renascent interests from both synthetic and materials research communities[1,2]. In particular, benefitted by the advanced synthetic techniques, an array of persistent, open-shell hydrocarbons has been achieved, displaying compelling potential for a range of applications that call for unique combinations of magnetic and opto-electronic properties[3–6]. Moreover, carbon-based polyradicals may present slow spin relaxation and depolarization capabilities, which are greatly valuable to the emerging fields of spintronics and quantum information technologies[7–9]. Among the various types of organic structures, π-conjugated scaffolds are especially apt platforms for devising multi-spin systems with tunable spin-spin interactions, because the readily tailorable polycyclic aromatic frameworks lend great convenience and flexibility to modulating the electron delocalization and spin orbital overlapping characteristics[10,11]. However, vast challenges prevail over the syntheses of high-spin organic molecules, because the chemo-stability of polyradicals deteriorates with increasing number of spins showing ferromagnetic (FM) coupling. While encouraging progress has recently been made with triplet diradicals[12–17], examples of stable, high-spin organic molecules with even more unpaired electrons remain sporadic[18–21]. Organic triradicals having a high-spin ground state of optimal stability reported so far are basically three types: carbon-centered, nitrogen-centered, and nitrogen oxide (NO) radicals. As NO radicals are rather localized, they mainly rely on through-space interactions for spin exchanges and typically display weaker spin coupling ($\Delta E_{D\text{-}Q} < 0.5$ kcal/mol)[22,23]. On the other hand, the carbon- and nitrogen-centered radicals, favored by more competent delocalization and orbital overlapping, may realize stronger FM coupling.

We are particularly interested in harnessing the outstanding π-delocalization ability of carbon radicals[10,15], because this unique

[1]Beijing National Laboratory for Molecular Sciences, Centre for the Soft Matter Science and Engineering, The Key Laboratory of Polymer Chemistry and Physics of the Ministry of Education, College of Chemistry, Peking University, Beijing, China. [2]Spin-X Institute, School of Chemistry and Chemical Engineering, Guangdong-Hong Kong-Macao Joint Laboratory of Optoelectronic and Magnetic Functional Materials, State Key Laboratory of Luminescent Materials and Devices, Guangdong Basic Research Center of Excellence for Functional Molecular Engineering, South China University of Technology, Guangzhou, China. [3]Quantum Science Center of Guangdong-Hong Kong-Macao Greater Bay Area, Shenzhen-Hong Kong International Science and Technology Park, Shenzhen, Guangdong, China. [4]These authors contributed equally: Xudong Bai, Di Zhang. ✉e-mail: jiangsd@scut.edu.cn; dhzhao@pku.edu.cn

property not only enhances the chemo-stability, but also avails stronger FM coupling and larger energy gaps between the low- and high-spin states ($\Delta E_{LS\text{-}HS}$), which is crucial to realizing reliable spin manipulations by suppressing thermally activated low-spin species. For example, in contrast to the previous triradicals devised with significant steric torsion around the non-Kekulé *m*-xylylene unit, which benefits the stability but hampers through-bond spin coupling[19,24], our recent design of a carbon-centered triradical[18], as well as the nitrogen-based triradicals developed by others[20,21], exploited large polycyclic π-skeletons to facilitate greater non-disjoint SOMO overlapping via delocalization, thereby attaining much stronger FM coupling and larger ΔE_{D-Q} (>1 kcal/mol).

[*n*]Triangulenes, a group of triangular polycyclic aromatic hydrocarbons (PAHs), are inherently imparted with high-spin, open-shell characters, due to the zig-zag nanographene edges[25–27]. Both Ovchinnikov's rule[28] and Lieb's theorem[29] suggest a continually increased number of unpaired electrons appearing in the progressively expanded triangulene framework (i.e., increasing *n*, Fig. 1). Importantly, all the unpaired spins are predicted by theory to be FM coupled[30,31] and therefore exhibit a high-spin ground state. While the smallest homolog, [2]triangulene (i.e., phenalenyl radical) is a well-known stable monoradical that has been synthesized and widely investigated (Fig. 1a)[32,33], larger triangulenes ($n = 3, 4, 5, 7$) are so far mostly prepared and studied in-situ on surfaces under high-vacuum conditions[34–37]. Their solution-phase syntheses and isolations are tremendously challenging, because these open-shell molecules become increasingly unstable with more net spins[38]. On the other hand, incorporating heteroatoms, such as B, N, O, or P, into the triangulene skeleton is shown to effectively modify the electronic properties and give rise to more stable closed-shell structures, some of which have realized functional applications as optoelectronic materials[39–42]. Nonetheless, the hetero-atom-embedded open-shell analogs with high-spin ground state still difficult to obtain. Most recently, the syntheses of [3]triangulene and aza[3]triangulene diradical cations bearing suitable steric-shielding groups are accomplished, and they are proven to have triplet ground states (Fig. 1a)[43–45]. Despite these advances, triangulene homologs of even larger size ($n \geq 4$) and higher spin quantum number ($S \geq 3/2$) remain elusive.

Here, we present the solution-phase synthesis of a stable 3,8,13-triaza[4]triangulene derivative (**1**), which possesses 3 net spins ($S = 3/2$) and thus a quartet ground state (Fig. 1b). Three nitrogen atoms are integrated to the periphery of the [4]triangulene scaffold in a C_3-symmetric manner. The purpose of such a molecular design is to enhance the chemo-stability of the polyradical, as our prior study indicated that introducing nitrogen atoms at suitable spin-sharing positions greatly helped stabilize the high-spin polyradicals compared with all-hydrocarbon analogs[16,18]. Additionally, steric-hindering *tert*-butyl (^{t}Bu) and 2,4,6-triisopropylphenyl (Tipp) groups are specifically installed around the triangular skeleton, which were as well shown indispensable to the stability of the high-spin species.

The pivotal steps involved in the synthesis of triaza[4]triangulene **1** feature a three-fold intramolecular Bischler-Napieralski annulation followed by Friedel-Crafts cyclization, to create a completely fused polycyclic scaffold, which is subsequently converted to the targeted triradical by oxidizing three C-H bonds to carbon radicals. Evidently, the π-conjugation capacity of [4]triangulene polycycle is critical to both the stability in ambient conditions ($\tau_{1/2}$ ~ 9 days for polycrystals stored in air and 28 h in an air-saturated solution) and pronounced FM exchange interactions manifested by **1**, as it allows the embedded spins to be extensively delocalized, bringing about significant non-disjoint

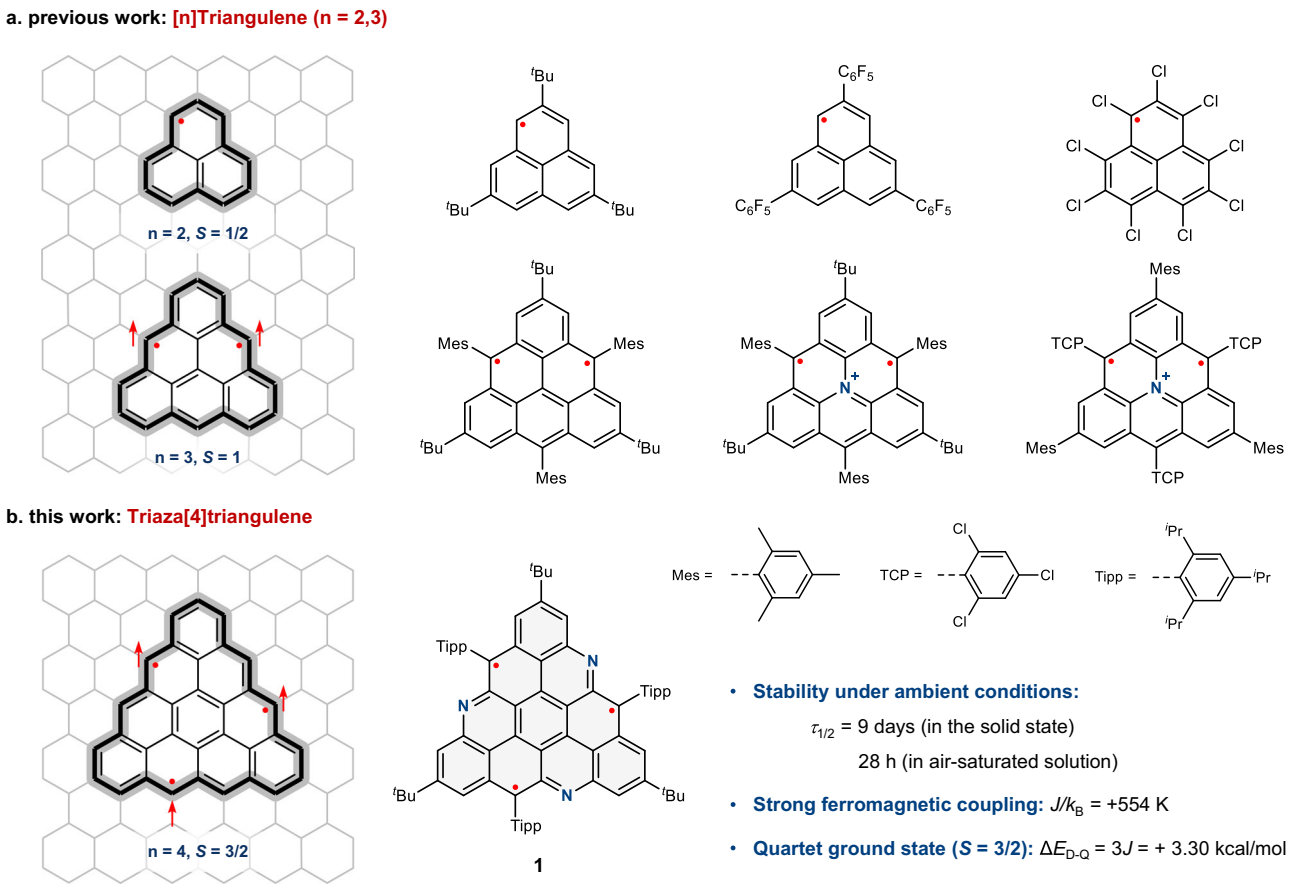

Fig. 1 | Solution-phase synthesized [*n*]triangulene radicals. a Previous examples of doublet [2]triangulenes, a triplet [3]triangulene, and triplet aza[3]triangulene diradical cations; **b** 3,8,13-triaza[4]triangulene **1** synthesized in the current work.

https://doi.org/10.1038/s41467-026-69048-1

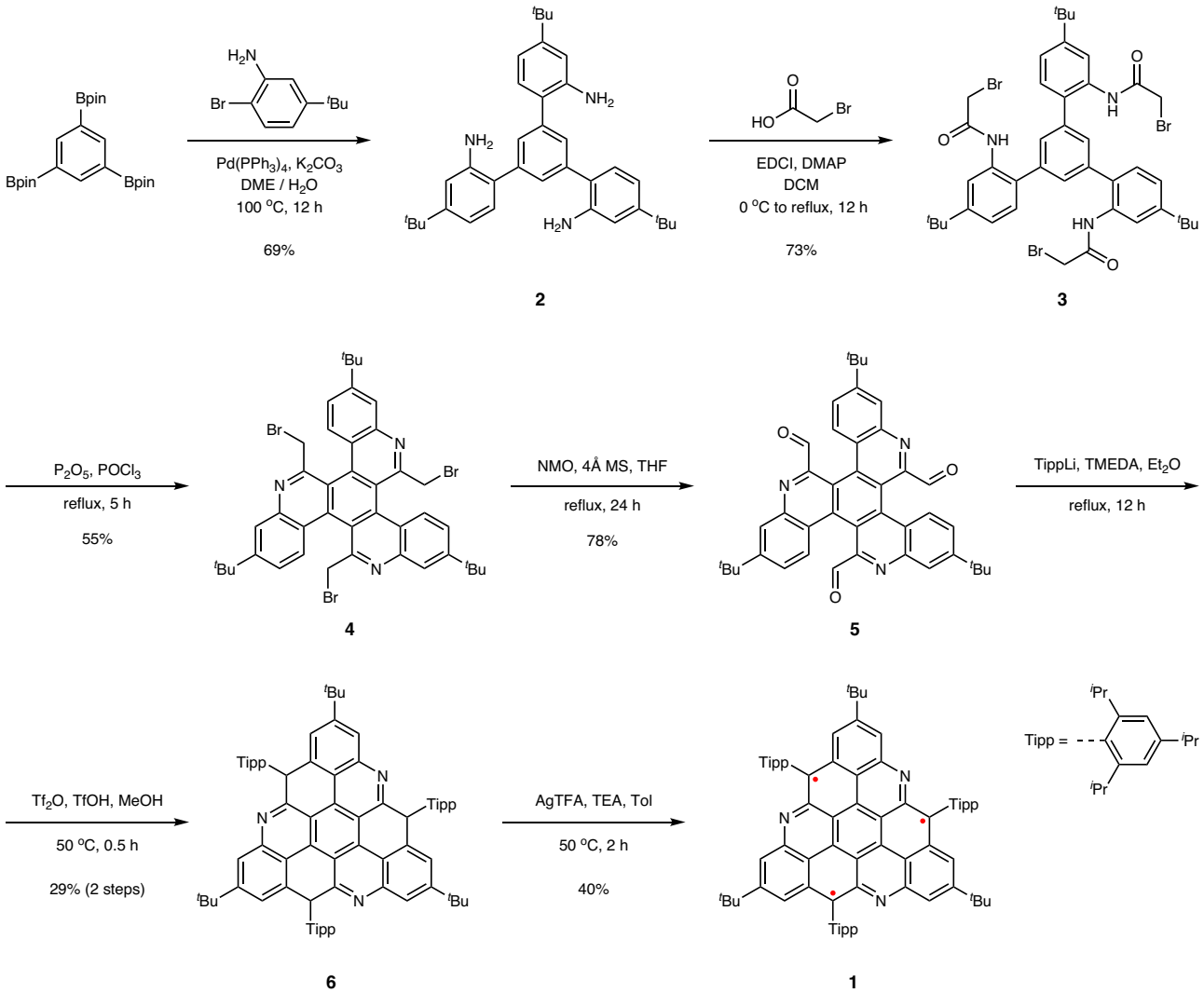

Fig. 2 | Synthetic route. Preparation steps and conditions of triradical **1**.

spin-orbital overlapping. The remarkable stability of **1** makes its isolation and complete characterization viable and facile. The triradical structure is confirmed by X-ray crystallography, and the quartet ground state is verified by various magnetic experiments. The hyperfine coupling behaviors unveiled by the electron paramagnetic resonance (EPR) spectra support the delocalized nature of the spins, and the superconducting quantum interference device (SQUID) identifies an extraordinary spin-spin coupling constant ($J/k_B = +534$ K, $\hat{H} = -2J(\hat{\boldsymbol{S}}_1 \cdot \hat{\boldsymbol{S}}_2 + \hat{\boldsymbol{S}}_2 \cdot \hat{\boldsymbol{S}}_3 + \hat{\boldsymbol{S}}_3 \cdot \hat{\boldsymbol{S}}_1)$), corresponding to a significant doublet-quartet energy gap ($\Delta E_{D\text{-}Q}$) of up to +3.18 kcal/mol by fitting to an equilateral triangle coupling model. Finally, impressive spin coherence and spin-lattice relaxation times ($T_m = 5.41$ µs and $T_1 = 11.3$ ms in toluene-d_8 at 20 K) are determined, and selective excitation between different Zeeman energy levels is also realized with the pulsed EPR technique, proving the suitable addressability of **1** for spin-manipulation experiments. As importantly, the synthetic protocol developed herein will greatly facilitate the developments of even larger (aza)[*n*]triangulenes.

Results and discussion

The synthesis of triradical **1** (Fig. 2) sets off from a triple Suzuki cross-coupling reaction, affording 1,3,5-tris(2-amino-4-*tert*-butylphenyl)benzene. Subsequently, upon amidation followed by Bischler-Napieralski annulation[46], a key intermediate consisting of three quinoline units centro-symmetrically fused to a benzene ring is produced. The appended bromomethyl groups are then converted to aldehydes, which subsequently undergo nucleophilic addition by lithiated triisopropylphenyl (Tipp). Next, the Friedel-Crafts cyclization is conducted with the resultant triol and offer the direct precursor to the triradical, from which targeted 3,8,13-triaza[4]triangulene **1** is obtained upon oxidation with silver(I) trifluoroacetate in the presence of triethylamine. The triradical molecule is found adequately stable to allow purification with column chromatography in the ambient air. Isolated **1** can be stored in N_2 atmosphere at room temperature for months without significant degradation. By monitoring the time-dependent decay of the EPR signal for **1** in an air-saturated toluene solution under ambient light and at room temperature, the half-life ($\tau_{1/2}$) was determined to be 28 h. In its polycrystalline form, the stability of **1** is significantly enhanced, with the $\tau_{1/2}$ increasing to 9 days (Supplementary Fig.7).

Single crystals suitable for X-ray crystallographic analyses are obtained by diffusing acetonitrile into a dichloromethane solution of **1** (CCDC 2379761) under a nitrogen atmosphere (Fig. 3 and Supplementary Table 1). The polycyclic skeleton of 3,8,13-triaza[4]triangulene is shown basically planar with C_3 symmetry, and all comprised C-C and C-N bonds fall in a narrow range of 1.365 to 1.431 Å. The nearly equalized bond lengths imply expected aromatic and extensive electron delocalization characteristics of the polycyclic moiety. Nearly

https://doi.org/10.1038/s41467-026-69048-1

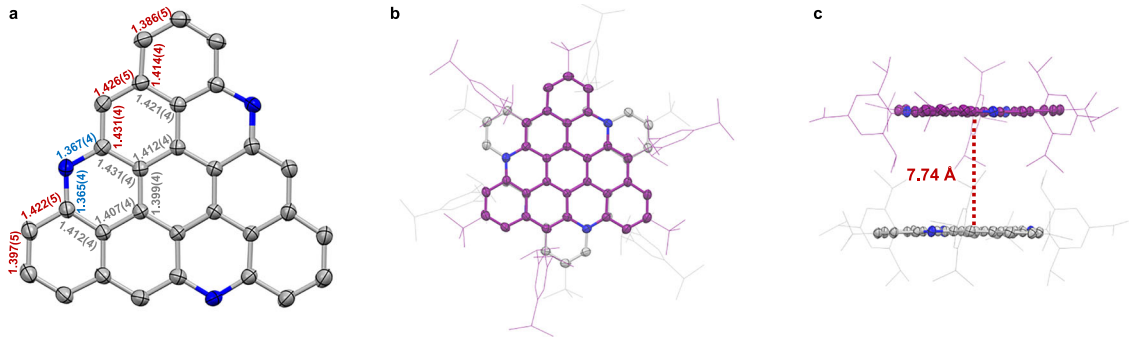

Fig. 3 | X-ray crystallographic structure of 1. a Structure of **1** with bond lengths and uncertainties in Å (bulky substituent groups and hydrogen atoms are omitted for clarity and displacement ellipsoids are drawn at the 30% probability level); **b**, **c** molecular packing viewed along the *c* and *a* axes.

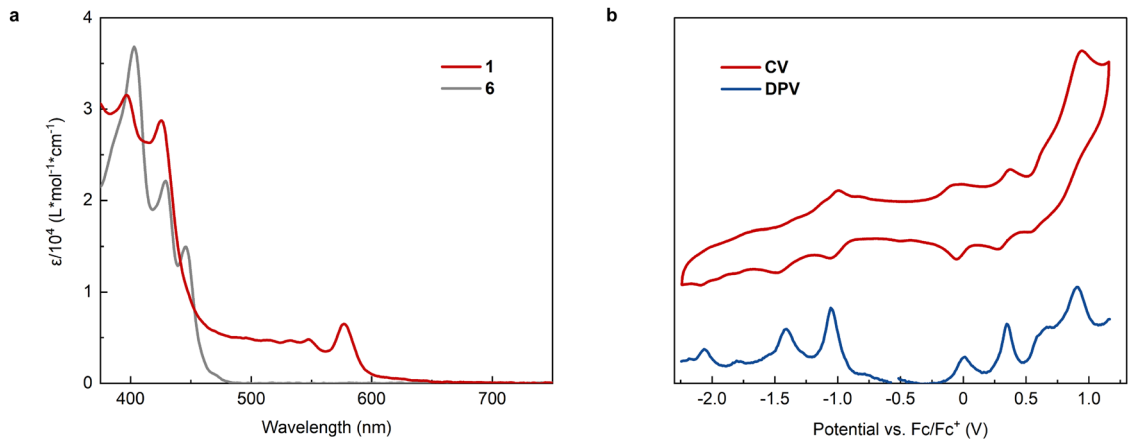

Fig. 4 | UV-vis absorptions and electrochemistry. a UV−vis absorption spectra of **1** (red) and precursor **6** (gray) in toluene; **b** Cyclic voltammetry (CV, red) and differential pulse voltammetry (DPV, blue) profiles of **1** in *o*-dichlorobenzene/acetonitrile with *n*-Bu_4NPF_6 (0.1 M) as the supporting electrolyte.

perpendicular dihedral angles (ca. 83°) are assumed by the Tipp groups with respect to the triangulene plane. Due to the steric hindrance conferred by the bulky Tipp and ^{t}Bu substituents installed around the planar polycyclic framework, which are crucial for protecting the triradical from intermolecular reactions, large inter-plane distances of ca. 7.7 Å, with a rotational angle of about 60°, are exhibited by adjacent triaza[4]triangulene π-skeletons, arranged into a semi-columnar packing motif (Figs. 3b and S2). With such long distances, the intermolecular spin-spin interactions are deemed negligible with crystalline **1**, and this conclusion is corroborated by the subsequent magnetic experiments.

The UV-Vis absorption spectrum of **1** is collected from its toluene solution (Fig. 4a). Compared with the trihydro- precursor **6**, the triradical presents an evident bathochromically shifted absorption band of medium intensity broadly ranging from 450 to 650 nm, which presumably arises from the aromatized π-framework and open-shell attributes of the triradical. TD-DFT computation indicates that this low-energy absorption of **1** primarily originates from its quartet state and can be ascribed to the transitions from multiple β-occupied orbitals to three β-SUMOs, thus giving rise to broad, overlapped peaks (Supplementary Figs. 13, 14 and Supplementary Table 3). Moreover, in contrast to the brightly emissive **6** (Supplementary Fig. 4), no fluorescence is detected from **1** at room temperature or 77 K, which is not surprising for a high-spin triradical. The cyclic voltammetry (CV) and differential pulse voltammetry (DPV) are performed in a mixed solvent of *o*-DCB and acetonitrile for improved solubility (Fig. 4b). Four consecutive oxidation and reduction waves are detected with **1**, purporting the multiple redox processes taking place with the triradical structure.

The investigation continued with a thorough analysis of the magnetic properties. In the continuous-wave (cw) EPR spectrum, **1** in deoxygenated toluene shows a resonance signal with complex yet well-resolved splitting pattern at room temperature (Fig. 5a), which can be simulated with three sets of nuclei associated with different hyperfine coupling constants (HFCCs) of 4.39 ($3\times{}^{14}$N), 6.72 ($3\times{}^{1}$H) and 6.61 ($3\times{}^{1}$H) MHz. Such splitting features can be reasonably attributed to the three equivalent ^{14}N atoms and two sets of three equivalent ^{1}H atoms appearing along the [4]triangulene periphery, coupled to the embedded spins. These HFCCs derived from the experimental data simulation are well consistent with the calculation results from the quartet state of **1**. Based on the relative magnitudes of calculated values, specific assignments of the three experimentally determined HFCCs to corresponding N and H atoms are made (Fig. 5c). When comparing these HFC properties of **1** with those of a monoradical **1′** with analogous structure (Supplementary Fig. 6), it is noted that not only the number of primary coupled nuclei increases by three times in the triradical, but the HFCC values decrease to roughly one third. These observations evidently prove that the three spins in **1** are delocalized and exchangeable in the triaza[4]triangulene framework. This conclusion is also fully agreed by the nearly equalized bond lengths revealed by the crystallography. The delocalization property is apparently favorable to the thermodynamic stability of the triradical.

In contrast to the isotropic signal detected with **1** at room temperature, resulting from the averaging effect of rapid molecular rotations, spin anisotropy emerges in frozen toluene at 77 K (Fig. 5b). The EPR signal broadens significantly, while an anisotropic *g*-factor ($g_x = g_y = 2.0032$, $g_z = 2.0026$) and pronounced zero field splitting (ZFS) feature are perceived, characteristic of $S = 3/2$ species. The ZFS

https://doi.org/10.1038/s41467-026-69048-1

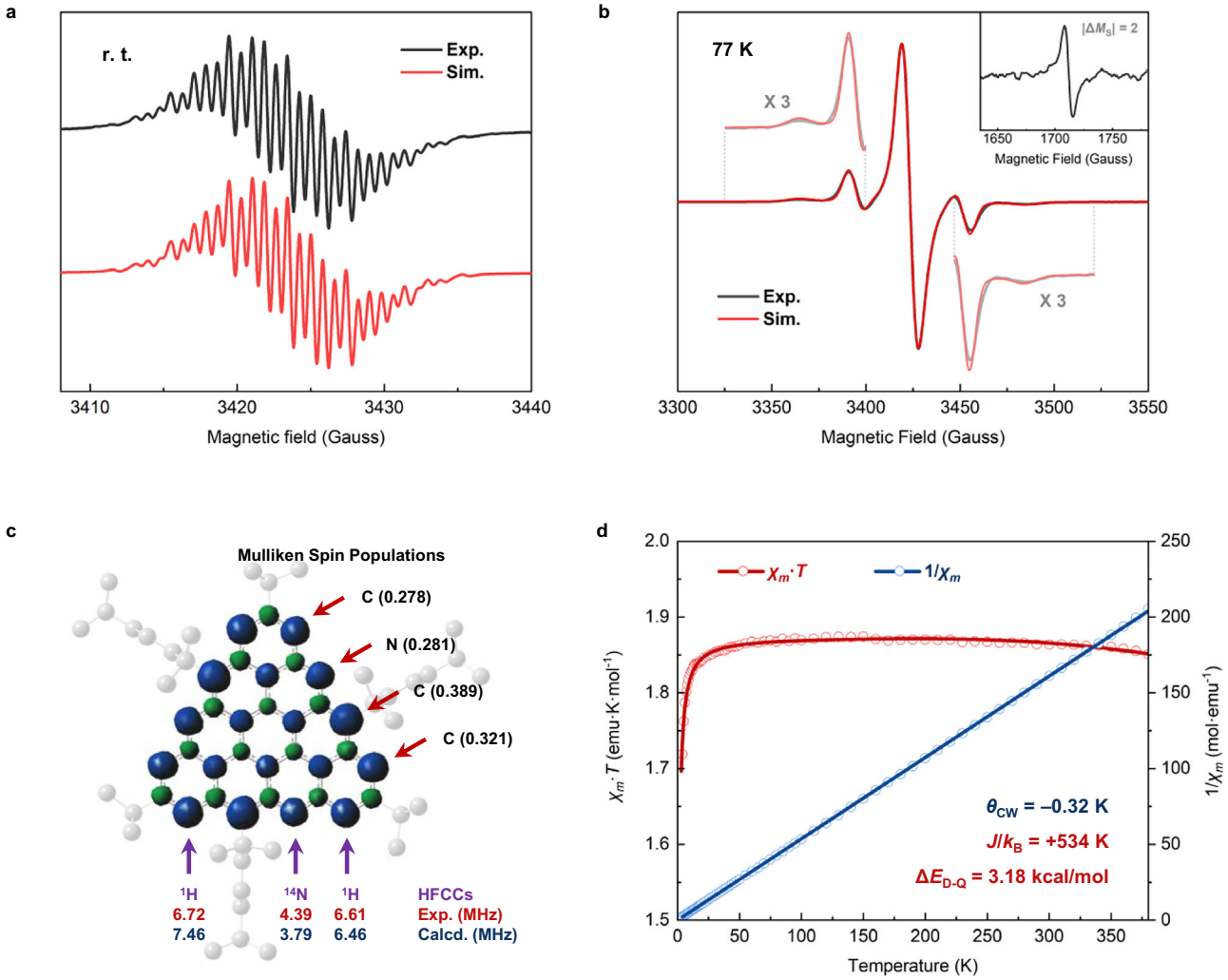

Fig. 5 | Magnetic characterizations. a cw-EPR spectrum of **1** in toluene at room temperature (gray) and simulation (red) using parameters of $S = 3/2$, $g = 2.0033$, $3\times A(^1\text{H}) = 6.72$ MHz, $3\times A(^1\text{H}) = 6.61$ MHz, $3\times A(^{14}\text{N}) = 4.39$ MHz; **b** cw-EPR spectrum of **1** in toluene at 77 K (gray) with overlaid simulation (red) using parameters of $S = 3/2$, $g_x = g_y = 2.0032$, $g_z = 2.0026$; $3\times A_{zz}$ (^{14}N) = 9.5 MHz; $|D| = 84.7$ MHz, $E = 0$; inset showing the half-field transition under the same condition; **c** calculated spin density distribution at UB3LYP-D3(BJ)/def2-TZVP level (atoms with significant Mulliken spin populations are labeled) and experimentally determined hyperfine coupling constants (HFCCs) from fitting the cw-EPR spectrum (red) in comparison to those calculated at UB3LYP/EPR-II level (blue); **d** SQUID measurement data (circles) from polycrystalline **1** and the best fitting curves (lines).

parameters are determined to be $|D| = 84.7$ MHz upon spectral simulation. Moreover, a half-field transition ($|\Delta M_S| = 2$) is detected at 77 K, providing additional evidence for the high-spin ground state of **1**. When **1** is dispersed in solid PMMA, very similar ZFS characteristics and anisotropic *g*-factors as shown by the frozen solution are manifested at room temperature, reasonably due to the suppressed molecular motions in the polymer matrix. The basically unchanged EPR signals in both frozen solution and solid matrix with varied temperatures (Supplementary Fig. 8) also indicate minimal disturbance of the thermally populated doublet to the ground quartet state and hence a considerable energy gap ($\Delta E_{D\text{-}Q}$) thereof.

To quantitatively analyze the spin-spin coupling strength in triaza[4]triangulene, the magnetic susceptibility profile is collected from polycrystalline **1** with SQUID. As shown in Fig. 5d, above the field-saturated zone (i.e., >30 K), the value of $\chi_m{\cdot}T$ remains roughly constant around 1.875 emu K mol^{-1} in a wide temperature range and decreases only slightly at higher temperatures, reaching a value of 1.865 emu K mol^{-1} around 300 K. As the theoretically predicted $\chi_m{\cdot}T$ for a $S = 3/2$ species is 1.875 emu K mol^{-1}, such magnetic susceptibility behaviors demonstrate a predominant quartet component in **1** with minimal thermal distribution to the doublet state, as well implying a sizable $\Delta E_{D\text{-}Q}$. Moreover, the χ_m^{-1}-T curve exhibits a linear relationship, revealing a Curie-Weiss temperature (θ_{CW}) of approximately –0.32 K. Such a small value suggests very weak intermolecular spin-spin interactions. Upon applying this value to the magnetic susceptibility relationship describing an the equilateral triangle model ($\hat{H} = -2J(\hat{\boldsymbol{S}}_1\cdot\hat{\boldsymbol{S}}_2 + \hat{\boldsymbol{S}}_2\cdot\hat{\boldsymbol{S}}_3 + \hat{\boldsymbol{S}}_3\cdot\hat{\boldsymbol{S}}_1)$ and Eq. (S3)), the spin-spin exchange coupling (J/k_B) of **1** is estimated to be +534 K, corresponding to a $\Delta E_{D\text{-}Q}$ of 3.18 kcal/mol. Remarkably, owing to the excellent thermal stability of **1**, no discernible decomposition is detected in the SQUID measurements, as evidenced by the nearly perfect linearity of the χ_m^{-1}-T curve up to 380 K, which allows for more accurate fitting of the very large energy gap. These values echo the numbers derived from the varied-temperature EPR experiments ($J/k_B = +624$ K, $\Delta E_{D\text{-}Q} = 3J = 3.72$ kcal/mol, Supplementary Fig. 9), highlighting particularly strong FM exchange coupling among organic triradicals[18–24].

Next, pulsed EPR is employed to further characterize the ground-state spin properties of **1**. In frozen toluene-d_8 at 20 K, the longest spin coherence time (T_m) is determined to be 5.41 µs at 3450 G, and the longest spin-lattice relaxation time (T_1) is determined to be 11.3 ms at

https://doi.org/10.1038/s41467-026-69048-1

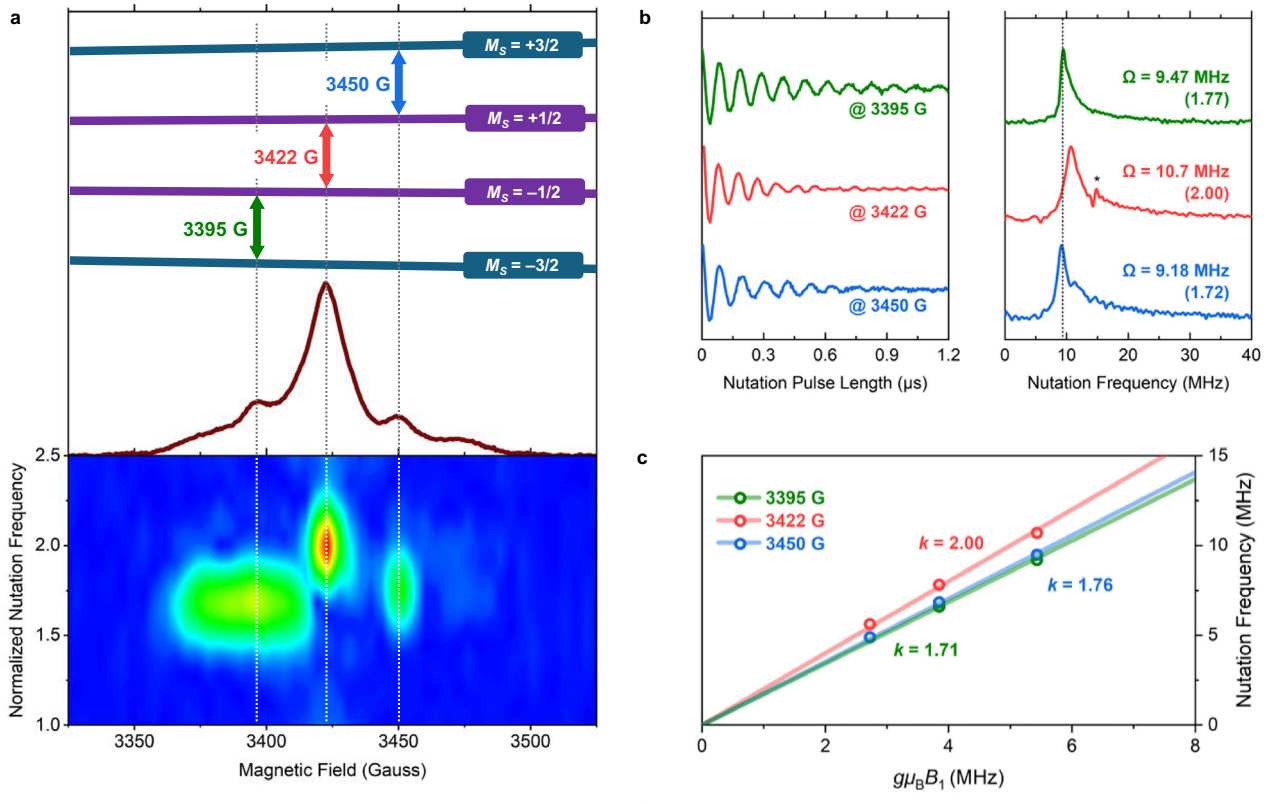

Fig. 6 | Pulsed EPR experiment results of 1. a EDFS and field-sweep 2D nutation spectra with the Zeeman energy level diagram (assuming $D > 0$); **b** electron spin nutation and Fourier transformation profiles at 9 dB power decay; **c** nutation frequency data (with fitting) showing linear dependence on the varied microwave field (B_1), exhibiting slope ratios (2:√3) characteristic of $S = 3/2$ species; all experiments are conducted in frozen toluene-d_8 at 20 K.

3395 G (Supplementary Fig. 10). Such desirably slow relaxation behaviors are deemed benefitted by the shape-persistent polycyclic skeleton that is rich in the non-magnetic ^{12}C atoms. This feature also renders a favorable signal-to-noise ratio in the subsequent pulsed experiments. The echo detected field sweep (EDFS) spectrum of **1** (Fig. 6a) presents very similar resonance peaks with those observed in the cw-experiment. Using the spin Hamiltonian derived from the spectrum simulation, the Zeeman energy diagram of **1** is delineated, and the resonance peaks are correlated to transitions between different Zeeman energy levels with respective M_S values (Supplementary Fig. 11). Basically, the transition in the center (at 3422 G) is designated as $|+1/2\rangle \leftrightarrow |-1/2\rangle$ in all *x*-, *y*- and *z*-directions of the magnetic field, and two resonance signals flanking the side are assigned to $|+3/2\rangle \leftrightarrow |+1/2\rangle$ and $|-1/2\rangle \leftrightarrow |-3/2\rangle$ in the *x*- and *y*-directions. Theoretically, under identical experimental conditions, the spin nutation frequencies of $M_S \leftrightarrow M_{S+1}$ transitions are proportional to $\sqrt{S(S+1) - M_S(M_S+1)}$ (Equation S2). Using the standard pulse sequence for Rabi oscillation, the spin nutation frequencies are then measured in different magnetic fields, while the microwave power is held constant at 9 dB. Upon transposing the time-domain signals to frequency-domain data via the Fourier transformation (Fig. 6b), the nutation frequency (10.7 MHz) recorded at 3422 G surpasses those detected at lower and higher fields of 3395 G (9.47 MHz) and 3450 G (9.18 MHz). By normalizing the frequency at 3422 G to a standard value of 2.00, the nutation frequencies at 3395 and 3450 G are calibrated to be 1.77 and 1.72, respectively, which are good approximations of the theoretical ratio of 2:$\sqrt{3}$. In the additional varied-microwave field power experiments (Fig. 6c), linear dependencies on the field power are exhibited and a slope ratio of 2:$\sqrt{3}$ is confirmed by the three sets of nutation frequencies resonating at different magnetic fields. These results unambiguously prove the spin nutation origin of the detected frequency. Moreover, the results from the 2D field-sweep nutation measurements (Fig. 6a) further confirm the 1D data, depicting well resolved peaks arising from different transitions. In addition to justifying the quartet ground state of **1**, these characterization results highlight the desirable addressability and thus impressive potentials of **1** in applications to the spin manipulation research as a four-level spin qu*d*it.

Finally, theoretical calculations are conducted to gain more insights into the spin properties of **1**. To avoid the spin contamination, a complete active space self-consistent field (CASSCF) method is first performed with the triaza[4]triangulene core without substituents, yielding $\Delta E_{D\text{-}Q} = 6.23$ kcal/mol at the level of CASSCF(7,7)/cc-pVTZ, as the computation cost for larger active spaces and entire molecule was overwhelming. The calculated $\Delta E_{D\text{-}Q}$ values based on different DFT methods (Supplementary Table 2) reveal that UB3LYP-D3(BJ)/def2-TZVP provides the best agreement with CASSCF. Thus, this method is selected for computations with the entire molecule. Using the single crystal structure as the initial form, the doublet and quartet states of **1** are optimized respectively (Supplementary Fig. 12) to give a $\Delta E_{D\text{-}Q}$ value of 6.59 kcal/mol. We deem that the quantitative discrepancy between the calculation and above experimental results likely originates from overestimated doublet-state energy by computation, which is typically caused by the spin contamination involved in unrestricted DFT calculations, as such a magnitude of difference falls in a similar range with those previously reported for alternative π-conjugated structures comprising delocalized spins showing ferromagnetic coupling behaviors[20,43–45].

By examining the frontier orbitals, three α-SOMOs are found to overlap significantly (Fig. 7a), depicting a prominent non-disjoint feature that is acknowledged to facilitate effective intramolecular FM spin exchanges[47]. These results provide a theoretic basis for the

https://doi.org/10.1038/s41467-026-69048-1

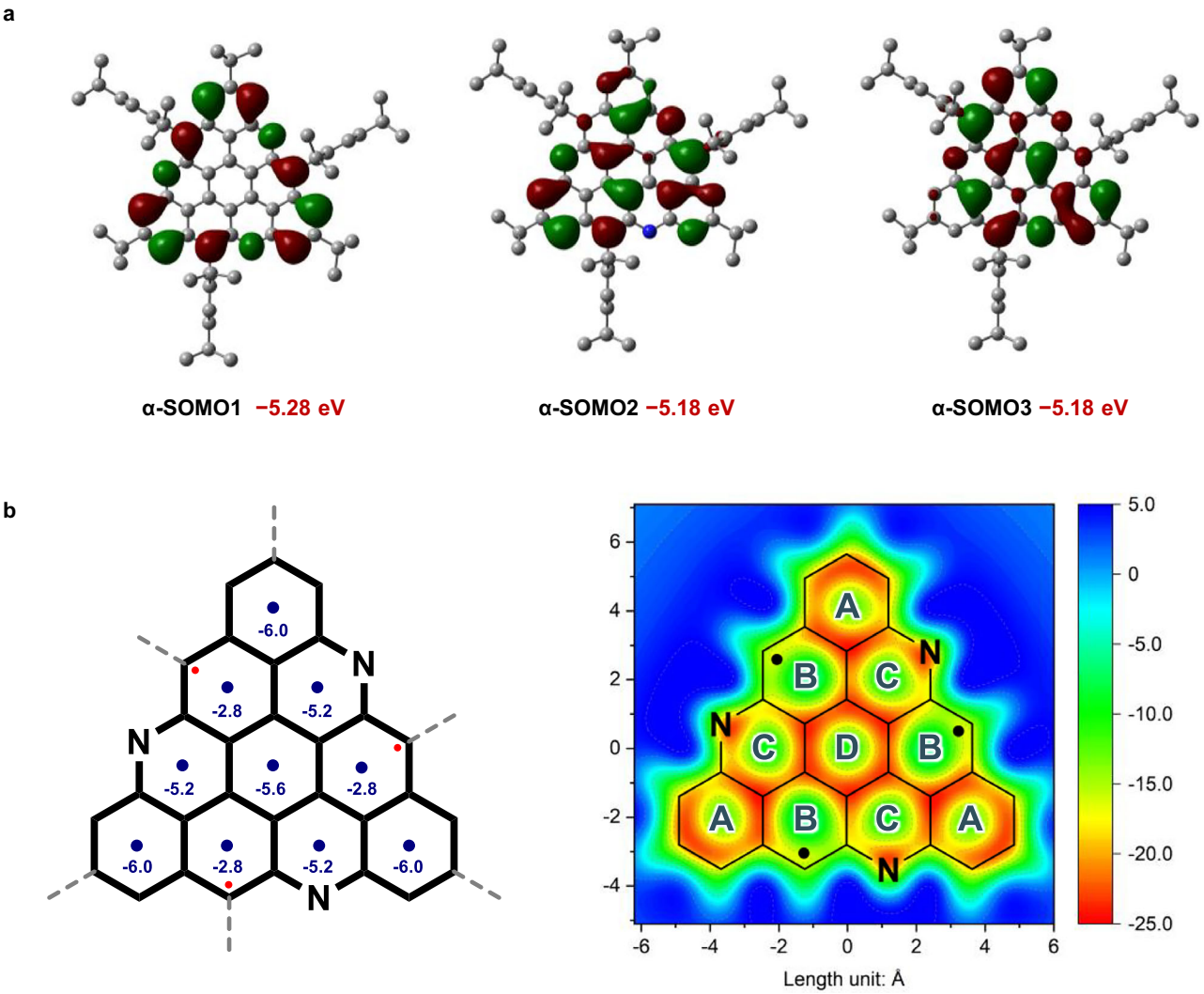

Fig. 7 | Theoretical calculations. a Frontier molecular orbitals of quartet **1** calculated at UB3LYP-D3(BJ)/def2-TZVP level; **b** NICS(1)$_{zz}$ values at the center of each aromatic ring and NICS(1)$_{zz}$ grids for quartet **1** with the substituents omitted.

experimentally determined very large $\Delta E_{D\text{-}Q}$ of **1**. The π-conjugation and aromaticity properties of 3,8,13-triaza[4]triangulene are then evaluated with the nucleus-independent chemical shift (NICS) calculations, which suggest that all hexagon rings present full conjugation, as evidenced by negative NICS(1)$_{zz}$ values. Compared with rings A and D, rings B and C display less negative NICS(1)$_{zz}$ values (Fig. 7b), and the former happens to possess slightly greater Mulliken spin populations (Fig. 5c). Moreover, the calculated spin density results show that the spin distribution in the 3,8,13-triaza[4]triangulene framework (Fig. 5c) is nearly identical to that found in the all-hydrocarbon [4]triangulene analog, proving that replacing the C(sp^2)-H units with isoelectronic N atoms does not significantly alter the spin distribution properties.

In summary, the solution-phase synthesis of a 3,8,13-triaza[4]triangulene derivative is successfully achieved in this work, which features a high-spin, quartet ground state yet impressive stability under ambient conditions ($\tau_{1/2}$ ~ 9 days in the solid state and 28 h in solution) as a triradical. The polycyclic triaza[4]triangulene skeleton is efficiently constructed through the Bischler-Napieralski reactions, to introduce the nitrogen atoms, allied with prior Suzuki couplings and followed by Friedel-Crafts cyclizations. Finally, oxidation of the three C(sp^3)-H bonds offers the aromatized triradical species. A number of factors such as the π-conjugated delocalization, *N*-heteroatom embedding, and bulky-substituent protection have all contributed to the favorable stability shown by the open-shell molecule. The single-crystal structure depicts large packing distances among the planar triangulene skeletons, implying negligible intermolecular spin-spin interactions. Continuous-wave and pulsed EPR spectroscopies offered conclusive evidence supporting the appearance of three highly delocalized, fully exchangeable spins, and especially the high-spin ground state, which includes the hyperfine coupling and zero-field splitting features, the half-field transition, and crucially, the spin nutation frequencies indicative of a quartet species. Quantitative measurements conducted with SQUID reveal a remarkable experimental value of 3.18 kcal/mol for $\Delta E_{D\text{-}Q}$, which is entailed by exceptionally strong intramolecular FM interactions evidenced by three equivalent extraordinarily spin-spin couplings (J/k_B = +534 K). Combined with suitable spin relaxation properties (T_m = 5.41 µs and T_1 = 11.3 ms in frozen toluene-d_8 at 20 K) and favorable addressability of quantum-state transitions as demonstrated by the pulsed EPR experiments, this quartet triradical represents as an attractive molecular material candidate for potential applications to the coherent spin manipulation studies.

Overall, this work provides a paradigm for designing and synthesizing stable, high-spin organic polyradicals that exhibit spin-manipulation properties favorable for developing molecular magnet materials, useful to the innovative technologies being developed in the

emerging fields of spintronics, quantum information processing, etc. Relevant synthetic efforts at further diversifying the structures of nanographene-based high-spin polyradicals are undertaken in our laboratory.

Methods

Synthesis of 6

1-Bromo-2,4,6-triisopropylbenzene (2.28 mL, 9.0 mmol) and distilled tetramethylethylenediamine (2.68 mL, 18.0 mmol) dissolved in anhydrous diethyl ether (45 mL) were cooled to 0 °C in an ice bath under N_2 atmosphere, to which *n*-BuLi (2.4 M in hexanes, 3.75 mL, 9.0 mmol) was added dropwise via a syringe. This mixture was stirred for 1 h at 0 °C before **5** (192 mg, 0.3 mmol) was added under a continuous flow of nitrogen gas. The reaction mixture was then slowly heated to 50 °C and stirred for 12 h. Upon cooling to room temperature, deionized water was added, and the resultant mixture was extracted with ethyl acetate. The organic layers were combined, washed with brine, dried over anhydrous Na_2SO_4, and concentrated under reduced pressure. The residue was purified using silica gel flash column (2 vol% ethyl acetate in dichloromethane), yielding the crude trihydroxy intermediate. Without further purification, this compound was transferred to a Schlenk tube. After evacuating and back-filling with nitrogen three times, a mixture of methanol, trifluoromethanesulfonic anhydride, and trifluoromethanesulfonic acid (10 mL, $v/v/v = 3:39:58$) was added, before the tube was sealed and heated at 80 °C for 1 h. After stirring at 50 °C for half an hour, the reaction mixture was cooled and poured into water. Upon careful neutralizing with saturated aq. $NaHCO_3$, extractions with dichloromethane were conducted and the organic layers were combined, washed with brine, dried over anhydrous Na_2SO_4 and then concentrated under reduced pressure. The residue was purified with silica gel column chromatography (10 vol% dichloromethane in petroleum ether), followed by recrystallization from methanol-dichloromethane, compound **6** was yielded as a yellow-green solid (103 mg, 29%).

Synthesis and isolation of 1

In a glove box, compound **6** (80 mg, 0.067 mmol) was dissolved in mixed anhydrous triethylamine and toluene (10 mL, $v/v = 1:10$), to which a solution of silver(I) trifluoroacetate (151 mg, 0.683 mmol) in anhydrous toluene (1 mL) was added. After stirring at 50 °C for 2 h, the reaction mixture became dark red and was removed from the glove box. The solvent was evaporated under reduced pressure and the residue was purified with flash column chromatography loaded with triethylamine-treated silica-gel (eluted with 8 vol% dichloromethane in *n*-hexane) to give **1** as a red solid (32 mg, 40%). The single crystals were grown by slowly diffusing acetonitrile into a dichloromethane solution of **1** under nitrogen atmosphere.

Data availability

All experimental details and data that support the findings of this study are included in this article and the Supplementary Information. Crystallographic data for the structures reported in this Article have been deposited at the Cambridge Crystallographic Data Centre, under deposition numbers CCDC 2379761 (**1**). Copies of the data can be obtained free of charge via https://www.ccdc.cam.ac.uk/structures/. All data are available from the corresponding authors upon request. Source data are provided with this paper.

References

1. Liu, B.-T. et al. Air-stable radical polycyclic aromatic hydrogen-bonded organic frameworks. *Chem* **11**, 102445 (2025).
2. Tahir, H. et al. Verdazyl radical polymers for advanced organic spintronics. *Nat. Commun.* **16**, 652 (2025).
3. Mizuno, A., Matsuoka, R., Mibu, T. & Kusamoto, T. Luminescent radicals. *Chem. Rev.* **124**, 1034–1121 (2024).
4. Cho, H.-H. et al. Efficient near-infrared organic light-emitting diodes with emission from spin doublet excitons. *Nat. Photon.* **18**, 905–912 (2024).
5. Wang, R. et al. Corral[n]bicarbazoles: redox-active chiral macrocycles for air-stable radical cations formation and guest capture/release. *Angew. Chem. Int. Ed.* **64**, e202511366 (2025).
6. Li, L., Prindle, C. R., Shi, W., Nuckolls, C. & Venkataraman, L. Radical single-molecule junctions. *J. Am. Chem. Soc.* **145**, 18182–18204 (2023).
7. Lombardi, F. et al. Synthetic tuning of the quantum properties of open-shell radicaloids. *Chem* **7**, 1363–1378 (2021).
8. Gorgon, S. et al. Reversible spin-optical interface in luminescent organic radicals. *Nature* **620**, 538–544 (2023).
9. Kopp, S. M. et al. Optically detected coherent spin control of organic molecular color center qubits. *J. Am. Chem. Soc.* **147**, 22951–22960 (2025).
10. Zhang, D. et al. Frustrated spins in π-conjugated triangular triradicals. *CCS Chem.* **7**, 1834–1843 (2025).
11. Han, H. et al. Aromatic stacking mediated spin-spin coupling in cyclophane-assembled diradicals. *J. Am. Chem. Soc.* **143**, 17690–17700 (2021).
12. Zhou, W. et al. Triplet-ground-state nonalternant nanographene with high stability and long spin lifetimes. *Nat. Commun.* **16**, 1006 (2025).
13. Jiao, T. et al. Solution-phase synthesis of Clar's goblet and elucidation of its spin properties. *Nat. Chem.* **17**, 924–932 (2025).
14. Wang, L. et al. Stable mono-radical and triplet diradicals based on allylic radical-embedded all-benzenoid polycyclic hydrocarbons. *Angew. Chem. Int. Ed.* **64**, e202415746 (2025).
15. Shu, C., Yang, Z. & Rajca, A. From stable radicals to thermally robust high-spin diradicals and triradicals. *Chem. Rev.* **123**, 11954–12003 (2023).
16. Zhu, Z. et al. Rational design of an air-stable, high-spin diradical with diazapyrene. *Angew. Chem. Int. Ed.* **62**, e202314900 (2023).
17. Shimizu, A. et al. Synthesis and isolation of a Kekule hydrocarbon with a triplet ground state. *Angew. Chem. Int. Ed.* **61**, e202205729 (2022).
18. Zhang, D. et al. An air-stable carbon-centered triradical with a well-addressable quartet ground state. *J. Am. Chem. Soc.* **146**, 21752–21761 (2024).
19. Veciana, J., Rovira, C., Ventosa, N., Crespo, M. I. & Palacio, F. Stable polyradicals with high-spin ground states. 2. Synthesis and characterization of a complete series of polyradicals derived from 2,4,6-trichloro-α,α,α′,α′,α″,α″-hexakis(pentachlorophenyl)mesitylene with S = 1/2, 1, and 3/2 ground states. *J. Am. Chem. Soc.* **115**, 57–64 (1993).
20. Zhang, H., Pink, M., Wang, Y., Rajca, S. & Rajca, A. High-spin S = 3/2 ground-state aminyl triradicals: toward high-spin oligo-aza nanographenes. *J. Am. Chem. Soc.* **144**, 19576–19591 (2022).
21. Shimizu, D. & Osuka, A. A benzene-1,3,5-triaminyl radical fused with Zn^{II}-porphyrins: remarkable stability and a high-spin quartet ground state. *Angew. Chem. Int. Ed.* **57**, 3733–3736 (2018).
22. Shu, C. et al. Synthesis and thin films of thermally robust quartet (S = 3/2) ground state triradical. *J. Am. Chem. Soc.* **143**, 5508–5518 (2021).
23. Tretyakov, E. V. et al. Platform for high-spin molecules: a verdazyl-nitronyl nitroxide triradical with quartet ground state. *J. Am. Chem. Soc.* **143**, 8164–8176 (2021).
24. Rajca, A. & Utamapanya, S. Poly(arylmethyl) quartet triradicals and quintet tetraradicals. *J. Am. Chem. Soc.* **115**, 2396–2401 (1993).
25. Zeng, W. & Wu, J. Open-shell graphene fragments. *Chem* **7**, 358–386 (2021).
26. Liu, J. & Feng, X. Synthetic tailoring of graphene nanostructures with zigzag-edged topologies: progress and perspectives. *Angew. Chem. Int. Ed.* **59**, 23386–23401 (2020).

27. Morita, Y., Suzuki, S., Sato, K. & Takui, T. Synthetic organic spin chemistry for structurally well-defined open-shell graphene fragments. *Nat. Chem.* **3**, 197–204 (2011).
28. Ovchinnikov, A. A. Multiplicity of the ground state of large alternant organic molecules with conjugated bonds. *Theor. Chim. Acta* **47**, 297–304 (1978).
29. Lieb, E. H. Two theorems on the Hubbard model. *Phys. Rev. Lett.* **62**, 1201–1204 (1989).
30. Yu, H., Sun, J. & Heine, T. Predicting magnetic coupling and spin-polarization energy in triangulene analogues. *J. Chem. Theory Comput.* **19**, 3486–3497 (2023).
31. Fernandez-Rossier, J. & Palacios, J. J. Magnetism in graphene nanoislands. *Phys. Rev. Lett.* **99**, 177204 (2007).
32. Ahmed, J. & Mandal, S. K. Phenalenyl radical: smallest polycyclic odd alternant hydrocarbon present in the graphene sheet. *Chem. Rev.* **122**, 11369–11431 (2022).
33. Uchida, K. & Kubo, T. Recent advances in the chemistry of phenalenyl. *J. Synth. Org. Chem. Jpn.* **74**, 1069–1077 (2016).
34. Pavlicek, N. et al. Synthesis and characterization of triangulene. *Nat. Nanotechnol.* **12**, 308–311 (2017).
35. Mishra, S. et al. Synthesis and characterization of pi-extended triangulene. *J. Am. Chem. Soc.* **141**, 10621–10625 (2019).
36. Mishra, S. et al. Synthesis and characterization of [7]triangulene. *Nanoscale* **13**, 1624–1628 (2021).
37. Su, J., Telychko, M., Song, S. & Lu, J. Triangulenes: from precursor design to on-surface synthesis and characterization. *Angew. Chem. Int. Ed.* **59**, 7658–7668 (2020).
38. Valenta, L. & Juricek, M. The taming of Clar's hydrocarbon. *Chem. Commun.* **58**, 10896–10906 (2022).
39. Chen, X. et al. 4]Triangulenes modified by three oxygen-boron-oxygen (OBO) units: synthesis, characterizations, and anti-kasha emissions. *J. Phys. Chem. Lett.* **13**, 10085–10091 (2022).
40. Chen, C. et al. Heteroatom-edged [4]triangulene: facile synthesis and two-dimensional on-surface self-assemblies. *Angew. Chem. Int. Ed.* **61**, e202212594 (2022).
41. Zhao, M. & Miao, Q. Design, synthesis and hydrogen bonding of B_3N_6-[4]triangulene. *Angew. Chem. Int. Ed.* **60**, 21289–21294 (2021).
42. Nakatsuka, S., Gotoh, H., Kinoshita, K., Yasuda, N. & Hatakeyama, T. Divergent synthesis of heteroatom-centered 4,8,12-triaza-triangulenes. *Angew. Chem. Int. Ed* **56**, 5087–5090 (2017).
43. Arikawa, S., Shimizu, A., Shiomi, D., Sato, K. & Shintani, R. Synthesis and isolation of a kinetically stabilized crystalline triangulene. *J. Am. Chem. Soc.* **143**, 19599–19605 (2021).
44. Arikawa, S. et al. A kinetically stabilized nitrogen-doped triangulene cation: stable and NIR fluorescent diradical cation with triplet ground state. *Angew. Chem. Int. Ed.* **62**, e202302714 (2023).
45. Wei, H. et al. Solution-phase synthesis and isolation of an aza-triangulene and its cation in crystalline form. *Angew. Chem. Int. Ed.* **61**, e202210386 (2022).
46. Chen, Y., Li, F. & Bo, Z. Facile synthesis of 3,8-dibromo-substituted phenanthridine derivatives and their conjugated polymers. *Macromolecules* **43**, 1349–1355 (2010).
47. Abe, M. Diradicals. *Chem. Rev.* **113**, 7011–7088 (2013).

Acknowledgements

The work is financially supported by the National Natural Science Foundation of China (No. 22431001 and 22175004, D. Zhao; No. 52503223, D. Zhang; No. 22488101, 22325503, and 22250001, S.J.), the Beijing National Laboratory for Molecular Sciences (BNLMS-CXXM-201902, D. Zhao), the Fundamental Research Funds for the Central Universities (2024ZYGXZR004, S.J.) and Guangdong Provincial Quantum Science Strategic Initiative (GDZX2301002, S.J.). The NMR and mass spectrometry measurements were performed at the Analytical Instrumentation Center of Peking University. The computational resources were supplied by the High-performance Computing Platform of Peking University.

Author contributions

D. Zhao and S.J. supervised the project. X.B., D. Zhang, and D. Zhao conceived the project, designed the research, and prepared the manuscript. X.B. and D. Zhang performed experiments and analyzed the data. Z.Z. provided suggestions for the molecule design. D. Zhang, Y.Z., and Y.W. contributed to the EPR measurements. D. Zhang and Y.X. contributed to the SQUID measurements. Y.C. contributed to the synthesis.

Competing interests

The authors declare no competing interests.

Additional information

Supplementary information The online version contains supplementary material available at https://doi.org/10.1038/s41467-026-69048-1.

Correspondence and requests for materials should be addressed to Shang-Da Jiang or Dahui Zhao.

Peer review information *Nature Communications* thanks the anonymous reviewers for their contribution to the peer review of this work. A peer review file is available.